RSC Advances

ROYAL SOCIETY OF CHEMISTRY

www.rsc.org/advances

Controllable hydrothermal synthesis of $Eu^{3+}/Tb^{3+}/Dy^{3+}$ activated $Zn_8[(BO_3)_3O_2(OH)_3]$ micro/nanostructured phosphors: energy transfer and tunable emissions

P. Liang [a], *J. W. Liu* [b] *and Z. H. Liu* [a, *]

A series of novel Tb^{3+}, Dy^{3+} single-doped and Eu^{3+}/Tb^{3+}, Tb^{3+}/Dy^{3+} co-doped $Zn_8[(BO_3)_3O_2(OH)_3]$(ZBH) micro/nano structured phosphors have been prepared under hydrothermal conditions without employing any template or surfactant. X-ray diffraction (XRD), scanning electron microscopy (SEM), field transmittance electron microscopy (FTEM) and photoluminescence spectroscopy (PL) and fluorescent decay times were used to characterize the as-prepared samples. The XRD, SEM and TEM results indicate that the doped concentration of RE (rare earth) ions can change the crystallinity and morphology of matrix. The PL results indicate that ZBH:Tb^{3+} is a good green phosphor. When co-doped the Eu^{3+} and Tb^{3+} ions into the ZBH matrix, the phosphor yielded tunable emissions including tri-band established white light emission based on the co-doped concentration and excitation wavelength, which was confirmed by the calculated Commission International de l'Eclairage chromaticity coordinates of Eu^{3+}/Tb^{3+} co-doped ZBH phosphors. When co-doped the Dy^{3+} and Tb^{3+} ions into the ZBH matrix, Tb^{3+} emission is sensitized by Dy^{3+} through a non-radiative resonant energy transfer, and there also exists energy transfer from matrix to Dy^{3+} under UV excitation including single-doped sample. The energy transferred from Tb^{3+} to Eu^{3+} ions, Dy^{3+} to Tb^{3+} and Tb^{3+} back to Dy^{3+} were controlled by selecting a suitable excitation wavelength, and the decay measurements were carried out for analyzing the energy transfer efficiency.

[a] *Key Laboratory for Macromolecular Science of Shaanxi Province, School of Chemistry and Chemical Engineering, Shaanxi Normal University, Xi'an 710100, People's Republic of China. E-mail: liuzh@snnu.edu.cn.*

[b] *School of Chemical and Biomedical Engineering, Nanyang Technological University, 62 Nanyang Drive, Singapore 637459, Singapore.*

†Electronic Supplementary Information (ESI) available: [This section includes the XRD patterns, SEM imagines of a series of ZBH:Dy^{3+}, ZBH:Eu^{3+}/Tb^{3+}, ZBH:Tb^{3+}/Dy^{3+},coordinated environments of two types of Zn^{2+} cations in ZBH, and photoluminescence properties of undoped ZBH and ZBH:0.05Eu^{3+}].

Introduction

In recent years, the phosphor has attracted increasing attention because of its applications in solid-state lighting, display devices, low-intensity IR imaging, watermarking technology, 3D storage media, solar cells and biological probes.[1] Phosphors are generally composed of microcrystalline host and luminescence activator formed by impurity metallic atoms intentionally incorporated.

In the case of host, many borates are chosen as host lattices for phosphors. According to others' work, the BO_3^{3-} radical in some borates has an absorption band in the range of 150–200 nm, and self-trapped excitons (STEs) show in the range of 300–350 nm.[2] Moreover, stability, convenient synthesis, and low cost are among the most desired properties of borates.[3] Among the borate materials, zinc borate is of most interest. It can be isolated as crystalline materials in various forms with different chemical compositions and structures, which can be categorized as hydrated zinc Borate, such as $Zn_8[(BO_3)_3O_2(OH)_3]$[4] and anhydrous zinc Borate such as ZnB_2O_4.[5] Anhydrous zinc borate as a host material doped with rare-earth ions such as Eu^{3+},[6] Tm^{3+},[7] Pr^{3+},[8] have been studied and shown excellent luminescent properties. But few studies about hydrous zinc borate as host material were reported,[10] since the –OH group and crystal water may decay the luminescent intensity. However, some researchers reported that hydrated borate based phosphors exhibited some superior luminescent properties to anhydrous borate based phosphors, such as higher color purity and lower preparation temperature, so hydrated borates could be a kind of new potential host for phosphors.[9-11]

In the case of metallic impurities, a large number of rare-earth ions have been used as the luminescence activators of phosphors, especially trivalent rare-earth ions that generally exhibit stable emission due to the f–f electron transition.[12] Tb^{3+}-doped phosphor is considered to be an attractive candidate for a gain medium in the green region around 540 nm since the $^5D_4$–$^7F_5$ transition of Tb^{3+} provides a four-level laser system allowing. In principle, Tb^{3+} as a green activator has lower threshold pump power compared to Er^{3+} ions[13] and shorter decay time than Mn^{2+} ion.[14] The work of searching novel phosphors with high luminescence efficiency is largely performed by two means. One approach is by quantum cutting (quantum splitting) or photon cascade emission (PCE). Another way is by sensitization, which is a traditional manner for enhancing the luminescence efficiency.[2] Among multitudinous sensitizer, Dy^{3+} ions can be activated by UV light, acting as good sensitizers and transferring part of their energy to other activator ions such as Tb^{3+}. Specifically, part of the energy in the $^4F_{9/2}$ level of Dy^{3+} is transferred to the $^5D_4$ level of Tb^{3+} by resonance between the two energy levels, so that the population in the terbium $^5D_4$ level is increased, resulting in enhancement green luminescence of the Tb^{3+}. Besides, the population in the $^5D_4$ level is also enhanced in detriment of that in the terbium $^5D_3$ level through cross-relaxation. Such cross relaxation mechanism induces an enhancement of the green luminescence from the terbium $^5D_4$ level at the expense of the luminescence violet–blue from the terbium $^5D_3$ level, transforming the light violet–blue into green, which is more sensitive to human eyes.[15] So, enormous efforts have been taken to fabricate the Tb^{3+} doped

borate materials through different methods. For example, A. Shyichuk et al. obtained Green-emitting nanoscale borate phosphors $Sr_3RE_2(BO_3)_4:Tb^{3+}$ by Pechini sol-gel method.[16] C. X. Qin et al. obtained one-dimensional Tb^{3+} doped $LaBO_3$ nanofiber through electrospinning method.[17] M. Manhas et al. synthesized gamma exposed $Ca_3B_2O_6:Tb^{3+}$ nanophosphor by combustion method.[18] F. X. Shan et al. prepared Tb^{3+}-doped $Na_3La_9O_3(BO_3)_8$ crystal by the top-seeded solution growth method.[19] J. Thakur et al. synthesized Eu^{3+} and Tb^{3+} doped $InBO_3$, $GdBO_3$ and $LaBO_3$ by glycine–nitrate combustion method.[20] D. Y. Wang et al. synthesized Tb^{3+}-doped $Ba_3Sc(BO_3)_3$ and investigate its Photo luminescence using synchrotron vacuum ultraviolet radiation.[21] J. Li prepared Tb^{3+}-doped $Zn(BO_2)_2$ phosphors by solid state reaction in the thermal carbon reducing atmosphere at high temperature.[22] H. H. Lin et al. synthesized $BaCaBO_3F:Ln^{3+}$ (Ln=Ce, Tb, Gd) and $BaCaBO_3F:Ce^{3+},Tb^{3+}$ and investigated their spectroscopic properties in the VUV–Vis range.[23] G. M. Cai et al. synthesized Tb^{3+}-activated $Li_3InB_2O_6$ through conventional solid-state reaction.[3a] But few researchers obtained RE doped borates through hydrothermal method.

So far, two methods are applied to obtain a WLED. One is to combine a blue LED chip and $YAG:Ce^{3+}$ yellow-emitting phosphor. The other is to fabricate a red–green–blue (RGB) emitting tri-phosphors excited by ultraviolet-LEDs. However, $YAG:Ce^{3+}$ yellow phosphor suffers some weaknesses, such as a poor color rendering index and low stability of color temperature. But for WLEDs, fabricated with ultraviolet-LED chips and tri-color phosphors, there still exists some problems that cannot be overcome so far. In particular, most of the above problems can be avoided by using single-phase white-emitting phosphors with excellent color rendering index. Meanwhile, the development of the single-phase white light emission materials may effectively solve the reabsorption problem existing in RGB phosphors. Numerous efforts have been made to achieve single-phase white-emitting luminescence materials based on Eu^{3+}, Eu^{2+}, Dy^{3+} single-doped and Tb^{3+}/Sm^{3+}, Tm^{3+}/Dy^{3+}, $Tm^{3+}/Tb^{3+}/Eu^{3+}$, $Yb^{3+}/Er^{3+}/Tm^{3+}$ co-doped.[24] According to literature, researchers usually get the white light emitting phosphors through adjusting Eu/Tb co-doped concentration, ratio and excitation wavelength. But rare studies focus on borates phosphor.[25] To the best of our knowledge, there is no repot about Eu^{3+}/Tb^{3+} co-doped in zinc borate aimed to obtain white light emitting phosphors.

In this paper, with an aim to develop new white-emitting and green-emitting phosphors, we select hydrous zinc borate ($Zn_8[(BO_3)_3O_2(OH)_3]$) as a host lattice with Tb^{3+}, Dy^{3+} single-doped and Eu^{3+}/Tb^{3+}, Tb^{3+}/Dy^{3+} co-doped. The results show that doped concentration of RE ions can change the crystallinity and morphology of ZBH. The energy transfer from Tb^{3+} to Eu^{3+} ions and host to Dy^{3+} and Dy^{3+} to Tb^{3+} were controlled by selecting a suitable excitation wavelength.

Experimental

Synthesis of samples

All of the reagents were of analytical grade and used directly without further purification.

For the synthesis of ZBH:xTb^{3+} (x=0.01, 0.03, 0.05, 0.07 and 0.10) samples, 6 mmol of $Zn(NO_3)_2 \cdot 6H_2O$ and the stoichiometric amounts of $Tb(NO_3)_3 \cdot 5H_2O$ were mixed in 30 mL distilled water forming solution A, and 3 mmol $NH_4HB_4O_7 \cdot 3H_2O$ dissolved in 30 mL distilled water at room temperature forming solution B. The solution B was dropwise added into solution A with constant stirring to form a homogenous mixture. After being stirred for 30 min at room temperature, the mixture was transferred to a 100 mL teflon-lined stainless steel autoclave, sealed, and maintained at 150 ^{o}C for 12 h, and then allowed to cool to room temperature naturally. The white precipitate was collected and washed several times with distilled water and absolute alcohol respectively, then dried at 60 ^{o}C for 12 h. The white powders of ZBH: Tb^{3+} microstructure were obtained.

For the synthesis of single doped ZBH:xDy^{3+} (x=0.01, 0.02, 0.03 and 0.04), co-doped ZBH:xEu^{3+}/yTb^{3+}(x=0.05; y=0.005, 0.01, 0.015 and 0.02) and ZBH:xTb^{3+}/yDy^{3+} (x=0.05; y=0.001, 0.005, 0.01 and 0.02) samples, the procedures were the same as stated above, but the stoichiometric amounts of $Tb(NO_3)_3 \cdot 5H_2O$ were replaced by stoichiometric amounts of $Dy(NO_3)_3 \cdot 6H_2O$, $Eu(NO_3)_3 \cdot 6H_2O$, and $Tb(NO_3)_3 \cdot 5H_2O$. The reproducibility of the synthesis of a series Tb^{3+}, Dy^{3+} single-doped and Eu^{3+}/Tb^{3+}, Tb^{3+}/Dy^{3+} co-doped ratio sample is high under this experiment conditions. The target emission of Tb^{3+} doped sample is green light, Dy^{3+} is blue, Eu^{3+}/Tb^{3+} is tunable from green to red, and Tb^{3+}/Dy^{3+} is tunable from green to blue.

As a comparison, the pure and undoped ZBH were also prepared as follows: 24 mmol of $NaBH_4$ dissolved in 30 mL distilled water forming solution A, and 6 mmol $Zn(Ac)_2 \cdot 2H_2O$ dissolved in 30 mL distilled water at room temperature forming solution B. The solution B was dropwise added into solution A with constant stirring to form a homogenous mixture. After being stirred for 30 min at room temperature, the mixture was transferred to a 100 mL teflon-lined stainless steel autoclave, sealed, and maintained at 150 ^{o}C for 12 h, and then allowed to cool to room temperature naturally. The white precipitate was collected and washed several times with distilled water and absolute alcohol respectively, then dried at 60 ^{o}C for 12 h. The white powders of pure and undoped ZBH microstructure were obtained.

Characterization

All samples were characterized by X-ray diffraction (XRD) (Rigaku D/max, operating at 40 kV and 30 mA, with Cu target at a scanning rate of 8 ^{o}/min, with 2θ range from 10 ^{o} to 50 ^{o}), scanning electron microscopy (SEM) (Quanta 200, Philips-FEI), field transmittance electron microscopy (FTEM) (Tecnai G2 F20, FEI) and thermogravimetric analysis (TGA) (performed on a TA-SDT Q600 thermal analyzer under N_2 atmosphere with a heating rate of 10 °C min^{-1} in the range of 30–1000 °C). The excitation and emission spectra were measured by F-7000(Hitachi) spectrophotometer equipped with a continuous 150 W Xenon lamp at room temperature. The lifetime and quantum efficiency (QE) were recorded using an FLS920P Edinburgh Analytical Instrument apparatus equipped with a 450 W xenon lamp and a μF900H high-energy micro-second flash lamp as the excitation sources.

Results and Discussion

Characterization of samples

Fig. 1 shows the XRD patterns of the undoped ZBH (a) and ZBH: xTb^{3+}(x=0.01, 0.03, 0.05, 0.07 and 0.10) (b-f), respectively. All the diffraction peaks could be perfectly indexed as the hexagonal phase ZBH (ICDD Card No. 97-041-6894), and no other impurities were detected. The doping of Tb^{3+} did not change the crystal structure of the product ZBH. The XRD patterns of the as-prepared samples ZBH:xDy^{3+} (x=0.01, 0.02, 0.03 and 0.04), ZBH:xEu^{3+}/yTb^{3+} (x=0.05; y=0.005, 0.01, 0.015 and 0.02), and ZBH:xTb^{3+}/yDy^{3+} (x=0.05; y=0.001, 0.005, 0.01 and 0.02) are shown in Fig. S1(A, B, C) in the Supporting Information. All samples show similar XRD patterns which are indexed as the ZBH (ICDD Card No. 97-041-6894). No other impurities can be observed. So, all the as-prepared samples are the single-phase. It is known that the ionic radii (r) of Zn^{2+} (CN = 4) and B^{3+} (CN = 3) are 0.74 Å and 0.21 Å, respectively. As the ionic radius of B^{3+} is too small, it is difficult for Eu^{3+} to replace B^{3+} in the ZBH. Hence, in this study, it is believed that the Zn^{2+} sites are partially substituted for Eu^{3+} in the lattice.

The effect of doped RE^{3+} concentration on the morphologies of the samples

The scan electron microscopes were used to present the morphologies of the samples. Seen from the SEM imagines in Fig. 2, the obtained undoped sample exhibited flower-like morphology, which was self-assembled by nanoplates with the thickness of about 100(±10) nm, as shown in Fig. 2a. The obtained sample with doped Tb^{3+} concentration of 1% exhibited microsphere morphology, which was self-assembled by nanoplates with the thickness of about 100(±10) nm, as shown in Fig. 2b. The obtained samples with doped Tb^{3+} concentration of 3% and 5% exhibited monodisperse microsphere morphology with a whirlpool, which was self-assembled by nanoplates with the thickness of about 300(±30) nm and 500(±50)nm, respecitively, as shown in Fig. 2c and 2d. Meanwhile, the 5% doped sample has a bigger volume and thicker nanoplates than 3% doped sample. The obtained sample with doped Tb^{3+}concentration of 7% exhibited bulk morphology, which was self-assembled by microplates with the thickness of about 1(±0.1) μm, as shown in Fig. 2e. The obtained sample with doped Tb^{3+} concentration of 10% exhibited silkworm-chrysalis-like, which was self-assembled by nanoplates with the thickness of about 200(±20) nm, as shown in Fig. 2f. It is obvious that the changes of Tb^{3+} doped concentration result in the different morphologies. The size of particles was measured with scanning electron microscopy coupled with Photoshop software.

The SEM images of the as-prepared samples ZBH:xDy^{3+} (x=0.01, 0.02, 0.03 and 0.04), ZBH:xEu^{3+}/yTb^{3+}(x=0.05; y=0.005, 0.01, 0.015 and 0.02) and ZBH:xTb^{3+}/yDy^{3+} (x=0.05; y=0.001, 0.005, 0.01 and 0.02) are shown in Fig. S2(A, B, C), respectively, in the Supporting Information. It is also obvious that the changes of Ln^{3+} (Ln=Tb, Dy and Eu) doped concentration result in the different morphologies. The TEM and HRTEM images of the as-prepared samples of ZBH:0.03Tb^{3+}, ZBH:0.01Dy^{3+}, ZBH:0.05Eu^{3+}/0.005Tb^{3+} and ZBH:0.05Tb^{3+}/0.001Dy^{3+} are shown in Fig. S3(a, b, c, d, e, f, g and h), respectively, in the Supporting Information. The inter-planar spacing of the as-prepared samples of ZBH:0.03Tb^{3+}, ZBH:0.01Dy^{3+}, ZBH:0.05Eu^{3+}/0.005Tb^{3+} and ZBH:0.05Tb^{3+}/0.001Dy^{3+} was

0.227 nm, 0.226 nm, 0.226 nm and 0.223 nm, respectively, which were very close to the d value (0.226 nm) of [214] faces in ZBH crystal.

For the kinetically driven shape controlled growth of nanocrystals, crystallographic phase of growth seeds and surface ligands that modulate surface energy of growing crystallites by selective adhesion are two important factors.[26] In the ZBH:Ln^{3+} (Ln=Tb, Dy and Eu) system, the Zn^{2+} sites in ZBH are partially occupied by the dopant ions. The imbalance of the electrical charges and the difference in the ionic radii between the host Zn^{2+} (0.74 Å nm) and the dopant Ln^{3+}(0.95−1.10 Å) ions lead to changes in the ion-to-ion distance and therefore spatial arrangement, local charge density, polarity and potential energy of specific crystal planes.[27] So, the introduction of Ln^{3+} ions in the reaction system may significantly influence the growth of the host lattices by modifying the crystallographic phase of the ZBH seeds at the primary growth stages, which eventually leads to doped nanocrystals with different morphologies. The presence of three valence Ln^{3+} ions instead of bivalence Zn^{2+} ions in the ZBH crystal is likely to enhance the adsorption of −OH ligands onto these basal surfaces. These ligands will prevent further extensive deposition of Zn^{2+} species at that surface.[28] Moreover, the increasing dopant concentration can heighten the changes in the ion-to-ion distance and therefore spatial arrangement, local charge density, polarity and potential energy of specific crystal planes, so, the relative concentration of dopant can also result in initial growth seeds with different crystallographic phases and shapes, which eventually lead to doped nanocrystals with different morphologies.

The UV excitation and emission spectra of ZBH:Tb^{3+}

The UV excitation spectra and the emission spectra under UV excitation for samples ZBH: xTb^{3+}(x=0.01, 0.03, 0.05, 0.07 and 0.10) were measured at room temperature. The excitation spectra of ZBH: xTb^{3+}(x=0.01, 0.03, 0.05, 0.07 and 0.10), taken with an emission wavelength of 546 nm, are shown in Fig. 3 (left). No remarkable difference on the spectroscopic characteristics was observed in the excitation spectra when different concentrations of Tb^{3+} ions were doped. Below the wavelength of 300 nm, the sharp band at 236 nm should correspond to the spin-allowed $4f^8 \rightarrow 4f^7 5d^1$ ($^7F_6 \rightarrow {}^7D$) transition of Tb^{3+}, and the broad band at 275 nm should correspond to the spin-forbidden $4f^8 \rightarrow 4f^7 5d^1$ ($^7F_6 \rightarrow {}^9D$) transition of Tb^{3+}.[14, 29] Weak excitation bands at 319, 341, 352, 370 and 380 nm correspond to the f-f transitions of Tb^{3+} in the host lattice. For all Tb^{3+} concentrations, the excitation spectra shapes are essentially the same except for intensity at different activator concentrations.

The emission spectra of ZBH:xTb^{3+} (x=0.01, 0.03, 0.05, 0.07 and 0.10) at room temperature (RT) are shown in Fig. 3 (right), which exhibit the same spectroscopic feature for different concentrations of Tb^{3+} ions in the samples. The spectra exhibit four main bands with the maxima at about 491, 546, 588, and 622 nm, which are due to the transitions from the excitation state $^5D_4$ to the ground states ^7F_J (J=6, 5, 4, 3) of Tb^{3+} in the host lattice. Among these transitions, the green emission located at 544 nm ($^5D_4 \rightarrow {}^7F_5$) is the strongest peak because it is a magnetic dipole allowed with $\Delta_J=\pm1$, so we can deduce that Tb^{3+} is located at a low symmetry site of Zn2 (as shown in Fig. S4 (right) in the Supporting Information) in the ZBH host lattices.[30] In addition, each emission is observed as two

sub-peaks, due to the Stark energy splitting, and it is influenced by the crystal field around Tb^{3+} ions in the host lattice.[31] The emission from $^5D_3$ level is not observed, suggesting the cross-relaxation ($^5D_3+^7F_6 \rightarrow ^5D_4+^7F_0$) of Tb^{3+} occurred in the concentration range we investigated.[25c, 32] For all Tb^{3+} concentrations, the emission spectra shape is essentially the same except for intensity at different activator concentration. With the concentration of Tb^{3+} increasing gradually, the emission associated with Tb^{3+} increases regularly before 7 mol% doped and then decreases because of the concentration quench. The corresponding CIE chromaticity diagrams for the emission spectra of the Tb^{3+} doped sample are shown in Fig. S5A.

The UV excitation and emission spectra of ZBH:Dy^{3+}

The excitation spectra of ZBH:xDy^{3+} (x=0.01, 0.02, 0.03 and 0.04) phosphors by monitoring the emission wavelength at 577 nm are shown in Fig. 4 (left). The spectra exhibit a broad absorption bands between 200 and 260 nm with the band maxima at 226 nm, and also exhibit the f–f transition of Dy^{3+} ion in the longer wavelength region. The broad band has been attributed to the O^{2-}–Dy^{3+} charge transfer band (CTB), which is caused by the electron transfer from 2p orbit of O^{2-} ion to 4f shell of Dy^{3+} ion. The f–f transition is assigned to the electronic transitions of ($^6H_{15/2} \rightarrow ^6P_{3/2}$) at 328 nm, ($^6H_{15/2} \rightarrow ^6P_{7/2}$) at 354 nm, ($^6H_{15/2} \rightarrow ^4P_{3/2}$) at 367 nm, ($^6H_{15/2} \rightarrow ^4I_{13/2}$) at 389 nm, ($^6H_{15/2} \rightarrow ^4G_{11/2}$) at 428 nm and ($^6H_{15/2} \rightarrow ^4I_{15/2}$) at 451 nm for Dy^{3+}.[33]

The emission spectra of ZBH:xDy^{3+} (x=0.01, 0.02, 0.03 and 0.04) phosphors when excited at 354 nm are shown in Fig. 4 (right). The spectra show emission in the blue region with the band maxima at 482 nm ($^4F_{9/2} \rightarrow ^6H_{15/2}$) and intense emission in the yellow region with the band maxima at 577 nm ($^4F_{9/2} \rightarrow ^6H_{13/2}$).[34] It is known that the $^4F_{9/2} \rightarrow ^6H_{15/2}$ transition belongs to the magnetic dipole transition, and it is hardly influenced by crystal field around Dy^{3+} ions, which is dominant if Dy^{3+} ions are in the inversion center. While the $^4F_{9/2} \rightarrow ^6H_{13/2}$ transition is corresponding to the forced electric dipole transition (ΔJ=2), which strongly varies with the chemical environment surrounding of Dy^{3+}.[31] Because the $^4F_{9/2} \rightarrow ^6H_{15/2}$ transition is not dominant, the Dy^{3+} is located at a low symmetry site of Zn2 in the ZBH host lattices. When the concentration of Dy^{3+} ions was increased above 3 mol%, the emission intensity decreased due to the concentration quenching. It is pointed out that the optimal concentration of Dy^{3+} ions is very small because of the cross-relaxation process through the resonance energy transfer between the neighboring Dy^{3+} ions. The energy of the $^4F_{9/2} \rightarrow ^6F_{11/2} + ^6H_{9/2}$ transition matches that of the $^6H_{15/2} \rightarrow ^6F_{11/2} + ^6H_{9/2}$ transition. Thus, with increasing concentration, the resonance energy transfer between the neighboring Dy^{3+} ions through cross-relaxation starts at dilute concentrations and is more frequent at higher concentrations.[33] In addition, the intensity of broad band from 400–500 nm gradually decreases with the increase of Dy^{3+} ion concentration. According to the excitation and emission spectra of ZBH:Dy^{3+}, the broad band originating from the borate hosts, as shown in Fig. S6 in supporting information, which can be attributed to the transition from the lower edge of the conduction to the upper edge of the valence band, called ‘‘band-gap’’ fluorescence.[35] The broad band is predominant of all emissions spectra monitored at the prominent characteristic excitation of Dy^{3+}, indicating that the doped Dy^{3+} cations can be excited through matrix absorption and the corresponding energy

transfer process is highly efficient. If a host itself emits and its emission overlaps with the direct absorptions of an activator (f–f or f–d transition), then non-radiation energy transfer from host to activator would happen according to the Forster–Dexter energy transfer theory.[21, 36] This suggests the ZBH is ideal host matrices for the luminescence of Dy^{3+}cations. The corresponding CIE chromaticity diagrams for the emission spectra of the Dy^{3+} doped sample are shown in Fig. S5B.

The UV excitation and emission spectra of ZBH:Eu^{3+}/Tb^{3+}

Fig. 5A shows the excitation spectra for the prepared phosphors ZBH:xEu^{3+}/yTb^{3+} (x=0.05; y=0.005, 0.01, 0.015 and 0.02) under emission wavelength at 544 nm. These excitation spectra are similar to those obtained for single doped ZBH: xTb^{3+} (Fig. 3 (left)). Below the wavelength 300 nm, a sharp band (~228 nm) can be observed, which should correspond to the spin-allowed $4f^8 \rightarrow 4f^7 5d^1$ ($^7F_6 \rightarrow {}^7D$) transition of Tb^{3+}. Weak excitation bands peaking at 320, 342, 353, 372 and 380 nm correspond to the f–f transitions of Tb^{3+} in the host lattice. Fig. 5B shows the excitation spectra for the prepared phosphors ZBH:xEu^{3+}/yTb^{3+} (x=0.05; y=0.005, 0.01, 0.015 and 0.02) under emission wavelength at 590 nm. These excitation spectra contain the characteristics of Eu^{3+} and Tb^{3+} in their respective single doped excitation spectra. The maximum peak at about 250 nm is ascribed to charge transfer band (CTB) from the 2p orbital of O^{2-} to the 4f orbital of Eu^{3+}. The peaks at 363 and 465 nm are ascribed to $^7F_0 \rightarrow {}^5D_J$ (J=4 and 2). The peaks at 318 nm, 381 nm, and 394 nm are ascribed to $^7F_0 \rightarrow {}^5H_3$, $^7F_0 \rightarrow {}^5L_7$, $^7F_0 \rightarrow {}^5L_6$ of Eu^{3+}. Meanwhile, a sharp band at about 228 nm should correspond to the spin-allowed $4f^8 \rightarrow 4f^7 5d^1$ ($^7F_6 \rightarrow {}^7D$) transition of Tb^{3+}. The peak at 371 nm is ascribed to $^7F_6 \rightarrow {}^5L_{10}$ of Tb^{3+}. And other peaks at 319, 341, 352 and 380 nm correspond to the f–f transitions of Tb^{3+} in the host lattice, which overlap with f-f transitions of Eu^{3+} and hardly be observed. Fig. 5C shows the excitation spectra for the prepared phosphors ZBH:xEu^{3+}/yTb^{3+} (x=0.05; y=0.005, 0.01, 0.015 and 0.02) under emission wavelength at 616 nm. These excitation spectra are similar to those obtained for single doped ZBH: xEu^{3+} (as shown in supporting information Fig. S7). The maximum peak at about 250 nm is ascribed to charge transfer band (CTB) from the 2p orbital of O^{2-} to the 4f orbital of Eu^{3+}. The peaks at 361 nm and 465 nm are ascribed to $^7F_0 \rightarrow {}^5D_J$ (J=4 and 2). The peaks at 318 nm, 381 nm, and 394 nm are ascribed to $^7F_0 \rightarrow {}^5H_3$, $^7F_0 \rightarrow {}^5L_7$, $^7F_0 \rightarrow {}^5L_6$ of Eu^{3+}. With the increases of Tb^{3+} ion concentration, the intensity of excitation spectrum corresponding to Eu^{3+} enhanced. So, we deduced that the energy can transfer from Tb^{3+} to Eu^{3+}.

Fig. 6A shows the emission spectra for the prepared phosphors ZBH:xEu^{3+}/yTb^{3+} (x=0.05; y=0.005, 0.01, 0.015 and 0.02) under 228 nm excitation. These emission spectra are similar to those obtained for single doped ZBH:xTb^{3+}. The emission spectra show two major peaks with respective regions at 490 nm ($^5D_4 \rightarrow {}^7F_6$) and 544 nm ($^5D_4 \rightarrow {}^7F_5$). With the content of Tb^{3+} enhancing gradually, the emission intensity associated with Tb^{3+} increases regularly. Fig. 6B shows the emission spectra for the prepared phosphor ZBH:xEu^{3+}/yTb^{3+} (x=0.05; y=0.005, 0.01, 0.015 and 0.02) under 245 nm excitation. These emission spectra contain the characteristic of Eu^{3+} and Tb^{3+} in their respective single doped emission spectra. The peaks at 491, 546, 588, and 622 nm are ascribed to the transitions from the excitation state $^5D_4$ to the ground states ^7F_J (J=6, 5, 4, 3) of Tb^{3+} in the host lattice. The peaks

at 590 and 616 nm are ascribed to the transitions from the excitation state $^5D_0$ to the ground states ^7F_J (J=1 and 2) of Eu^{3+} in the host lattice. Fig. 6C shows the emission spectra for the prepared phosphors ZBH:xEu^{3+}/yTb^{3+} (x=0.05; y=0.005, 0.01, 0.015 and 0.02) under 394 nm excitation. Except the Eu^{3+} and Tb^{3+}emission spectra, there have the host emission spectra. In Fig. 6B, the characteristic emission peaks of Eu^{3+} at 590 and 616 nm can be regularly enhanced with the increase of Tb^{3+} concentration gradually when the Eu^{3+} concentration is fixed. But in Fig.6C, the characteristic peaks of Eu^{3+} at 590 and 616nm can be enhanced before 1 mol% Tb^{3+} ions doped and then decreased because of the concentration quench. So, we speculate that there exists energy transfer from Tb^{3+} to Eu^{3+} ions.

In the ZBH:xEu^{3+}/yTb^{3+} (x=0.05; y=0.005, 0.01, 0.015 and 0.02) phosphors, the blue, green and red emission bands can be excited by UV light simultaneously in the ZBH:xEu^{3+}/yTb^{3+} phosphors, and the emission intensity can be adjusted by changing the excitation wavelength and relative doping concentrations of the Eu^{3+} and Tb^{3+} ions, so the luminescence color can be changed by varying the excitation wavelength, too. The result can be confirmed by the corresponding CIE chromaticity diagram for the emission spectra of the Eu^{3+} and Tb^{3+}co-doped ZBH:xEu^{3+}/yTb^{3+} samples, as shown in Fig. 7. In Fig. 7A, the color of ZBH:xEu^{3+}/yTb^{3+} (x=0.05; y=0.005, 0.01, 0.015, 0.02) phosphor gradually changed from white to green under the excitation of 245 nm, with the gradually increasing concentration of Tb^{3+}. And calculated CIE coordinate of the white emission is (0.337, 0.290). Meanwhile the color of ZBH:xEu^{3+}/yTb^{3} phosphor can be adjusted by changer the UV excitation wavelength. For instance, the color of ZBH:0.05Eu^{3+}/0.005Tb^{3+} phosphor is green (0.204, 0.293) under excitation of 228nm, white (0.337, 0.290) under 245nm excitation, and also white (0.314, 0.332) under excitation of 394 nm, as shown in Fig. 7B. This result indicates that the as-obtained phosphors could show merits of multicolor emissions in the visible region when excited by multi-wavelength light, which might find potential applications in the fields such as light display systems and watermarking technology.

The photoluminescence decay curves of the ZBH:0.05Eu^{3+} and ZBH:0.05Eu^{3+}/0.005Tb^{3+}phosphors were also investigated, which indicate that all the curves can be well fitted into a linear function as $\ln(I(t))=\mathrm{Ln}(I_0)+(-t/\tau)$, where ln(I(t)) is the emission intensity at time t, $\ln(I_0)$ is constant, τ is the decay lifetime, respectively. The lifetimes are measured to be 1.027 ms and 0.910 ms for ZBH:0.005$Tb^{3+}$and ZBH:0.05Eu^{3+}/0.005Tb^{3+} samples of Eu^{3+} (λ_{ex}=245 nm, λ_{em}=616 nm), respectively (Fig. 8A). The lifetimes are measured to be 0.426 ms and 0.475 ms for ZBH:0.05$Eu^{3+}$and ZBH:0.05Eu^{3+}/0.005Tb^{3+} samples of Eu^{3+} (λ_{ex}=245 nm, λ_{em}=616 nm), respectively (Fig. 8B). This decreased decay time in Eu^{3+}/Tb^{3+} co-doped sample of $Tb^{3+}$and increased decay time in Eu^{3+}/Tb^{3+} co-doped sample of Eu^{3+} evidently illustrates the fact that energy is transferred from Tb^{3+} to Eu^{3+}. A simple experimental formula can be used to estimate the $Tb^{3+}\rightarrow Eu^{3+}$ energy-transfer efficiency ($\eta_{Dy\rightarrow Tb}$):[29]

$$H_{Tb\rightarrow Eu}=1-\tau/\tau_0 \qquad (1)$$

where τ_0 and τ are the Tb^{3+} donor lifetimes in the absence and presence of Eu^{3+} acceptor respectively.

According to the above formulas (1), the values of $\eta_{Tb\rightarrow Eu}$ can be calculated as 0.114. Moreover, the quantum efficiency of sample (ZBH:0.05Eu/0.005Tb) under 254 nm excited is about 3.31%.

The energy transfer possibility from Tb^{3+} to Eu^{3+} ions in the PL process is presented in Fig. 9. First, electrons on Tb^{3+} ions are excited from the ground state ($4f^8$) to the excited state ($4f^75d$) by UV light. Subsequently, these electrons relax to the lowest excited state $^5D_4$ through multi-phonon relaxation then either return to the ground state to produce the Tb^{3+} emissions ($^5D_4\rightarrow{}^7F_{6,\ 5,\ 4,\ 3}$). Meanwhile, the energy transfer can occur from the f–d transition of Tb^{3+} ions at high energy levels to the next level f–f transition of Eu^{3+} excitation states (i.e. the energy transfer from the low spin f–d transition (228 nm) to the $^5I_4$ f–f transition of Eu^{3+} ions and the high spin f–d transition (275 nm) to the $^5F_3$ excitation level of Eu^{3+} ions). Finally, the energy is transferred non-radioactively to the $^5D_0$ metastable state, and cross-relaxation process occurs between the $^5D_3$, $^5D_4$ emission levels of Tb^{3+} ions and $^7F_0$, $^7F_1$ excitation levels of Eu^{3+} ions, because they are well overlapped with each other. Thus, when excited with photons, one possible way of energy transfer is via the $^7F_0\rightarrow{}^5I_4$ f–f transition of Eu^{3+} ions.

The UV excitation spectra and the emission of ZBH:xTb^{3+}/ yDy^{3+}

Fig. 10A and 10B show the excitation spectra of ZBH: xTb^{3+}/yDy^{3+}(x=0.05; y=0.001, 0.005, 0.01 and 0.02) obtained by monitoring the emissions at 544 nm and 577 nm, respectively. As shown in Fig. 10A, the observed peaks for ZBH: xTb^{3+}/yDy^{3+} under emission of 544 nm are similar to those obtained for single doped ZBH: xTb^{3+} (Fig. 3 (left)). Below the wavelength 300 nm, a sharp band (~228 nm) can be observed, which should correspond to the spin-allowed $4f^8\rightarrow4f^75d^1$ ($^7F_6\rightarrow{}^7D$) transition of Tb^{3+}. Weak excitation bands peaking at 319, 341, 352, 370 and 380 nm correspond to the f–f transitions of Tb^{3+} in the host lattice. As shown in Fig. 10B, the observed peaks for ZBH: xTb^{3+}/yDy^{3+} (x=0.05; y=0.001, 0.005, 0.01 and 0.02) under emission of 577 nm are similar to those obtained for single doped ZBH: xDy^{3+} (Fig. 4 (left)). The spectra exhibit a broad absorption band between 200 and 260 nm with the band maxima at 226 nm and the f–f transitions of Dy^{3+} ions in the longer wavelength regions. The broad band has been attributed to the O^{2-}–Dy^{3+} charge transfer band (CTB). The f–f transitions are assigned to the electronic transitions of ($^6H_{15/2}\rightarrow{}^6P_{3/2}$) at 328 nm, ($^6H_{15/2}\rightarrow{}^6P_{7/2}$) at 354 nm, ($^6H_{15/2}\rightarrow{}^4P_{3/2}$) at 367 nm, ($^6H_{15/2}\rightarrow{}^4I_{13/2}$) at 389 nm, ($^6H_{15/2}\rightarrow{}^4G_{11/2}$) at 428 nm and ($^6H_{15/2}\rightarrow{}^4I_{15/2}$) at 451 nm for Dy^{3+}.

Fig. 11A shows the emission spectra of ZBH:xTb^{3+}/yDy^{3+} (x=0.05; y=0.001, 0.005, 0.01 and 0.02) with 233 nm excitation wavelength. The spectra pertaining to the single doped Tb^{3+} ions exhibits emission peaks at 491 nm, 546 nm, 588 nm and 622 nm corresponding to the $^5D_4\rightarrow{}^7F_J$ (J=6, 5, 4, 3) transitions, respectively. And the emission spectra of Dy^{3+} can hardly be found under the 233 nm excitation. We conclude that the dosage of Dy^{3+} is so small that its emission spectrum is too low to be observed. On the other hand, the spectra of co-doped Tb^{3+}/Dy^{3+} ions, excited by 353 nm, exhibit the additional emission bands from the excited $^4F_{9/2}\rightarrow{}^6H_{13/2}$ level of Dy^{3+} ion, as shown in Fig. 11B. The $^4F_{9/2}\rightarrow{}^6H_{15/2}$ level of Dy^{3+} overlaps with the $^5D_4\rightarrow{}^7F_6$ level of Tb^{3+}. Meanwhile, the hump band between 400-475 nm could be ascribed to host emission spectra. In particular, the enhancing intensity of green emission band at 546 nm has been noticed with the increasing concentration of Dy^{3+} ions from

0.1 mol% to 1 mol%, as shown in Fig. 11A and B. The efficiency of the energy transfer from Dy^{3+} to Tb^{3+} ions can be quantified as a function of increasing concentration of Dy^{3+} ions, and the resonance energy transfer (RET) through cross-relaxation from Dy^{3+} to Tb^{3+} ions could be listed as: Dy^{3+} ($^4F_{9/2}$) + Tb^{3+}($^7F_6$)→Dy^{3+} ($^6H_{15/2}$) + Tb^{3+}($^5D_4$).[37] The intensity of green emission band at 546 nm decreased with further increasing the Tb^{3+} ion concentration from 1 mol% to 3 mol%. This may be due to the concentration quench. The corresponding CIE chromaticity diagrams for the emission spectra of the Tb^{3+}/Dy^{3+} co-doped sample are shown in Fig. S5C.

The photoluminescence decay curves of the ZBH:0.05Tb^{3+}, ZBH:0.01Dy^{3+} and ZBH:0.05Tb^{3+}/0.01Dy^{3+} phosphors were also investigated, as shown in Fig. 12. The decay curves of the ZBH:0.05Eu^{3+} and ZBH:0.05Eu^{3+}/0.005Tb^{3+} samples indicate that all the curves can be well fitted into a linear function. The lifetimes are determined to be 1.47 ms and 1.25 ms for ZBH:0.05Tb^{3+} and ZBH:0.05Tb^{3+}/0.01Dy^{3+} samples of Tb^{3+} (λ_{ex}=228nm, λ_{em}=545nm), respectively. The lifetimes are determined to be 0.158 ms and 0.122 ms for ZBH:0.01Dy^{3+} and ZBH:0.05Tb^{3+}/0.01Dy^{3+} samples of Dy^{3+} (λ_{ex}=353nm, λ_{em}=577nm) respectively (Fig. 8). This decreased decay times of Tb^{3+} and Dy^{3+} in Tb^{3+}/Dy^{3+} co-doped sample compared to their single-doped samples, respectively, can be treated as a strong evidence that energy is mutual-transferred between Tb^{3+} and Dy^{3+}. A simple experimental formula can be used to estimate the Dy^{3+}→Tb^{3+} energy-transfer efficiency ($\eta_{Dy\rightarrow Tb}$):[29]

$$\eta_{Dy\rightarrow Tb}=1-\tau/\tau_0 \qquad (2)$$

where τ_0 and τ are the Dy^{3+} donor lifetimes in the absence and presence of Tb^{3+} acceptor respectively. According to the above formulas (1), the values of $\eta_{Dy\rightarrow Tb}$ and $\eta_{Tb\rightarrow Dy}$ can be calculated as 0.185 and 0.196 of ZBH:0.05Tb^{3+}/0.01Dy^{3+}, respectively.

The possible energy transfer process between Dy^{3+} and Tb^{3+} is depicted in Fig. 13. Firstly, the electrons of the hosts are first excited from the ground state to the excited state after absorbing the UV light. Subsequently, the electrons in the excited state can either relax to the lowest ground state of ZBH, or transfer the excited energy to the level of $^4F_{9/2}$ or higher levels in Dy^{3+} through a resonance process.[38] Then, Dy^{3+} ions can transfer $^4F_{9/2}$ level energy to $^5D_4$ level of Tb^{3+} ions, and $^5D_3$ level energy of Tb^{3+} can transfer back to $^4F_{7/2}$ level of Dy^{3+} ions.[15] The energy through non-radiative relax from high energy level to the lower excited energy level by multi-phonon relaxation. The multi-phonon relaxation can increase the accumulated number of rare-earth ions on the metastable energy level, and then affect their luminescent efficiency. On the other hand, the Dy^{3+} and Tb^{3+} ions can also be excited by their own typical f–f transitions.

Moreover, the thermal stability of ZBH had been studied. The TG curve in Fig. S8 indicates that this product is stable up to about 350 °C and then begins to decompose after this temperature.

Conclusions

In summary, we have successfully synthesized lanthanide ions (Eu^{3+}, Tb^{3+}, Dy^{3+}) activated $Zn_8[(BO_3)_3O_2(OH)_3]$

nanostructured phosphors. The XRD and SEM results indicate that the doped concentration of RE ions can change the crystallinity and morphology of matrix. The PL results indicate that ZBH:Tb^{3+} is a good green phosphor, and the ZBH: Eu^{3+}/Tb^{3+} phosphor yields tunable emissions including tri-band established white light emission based on the co-doped concentration and excitation wavelength. The energy transfers from Tb^{3+} to Eu^{3+} ions, Dy^{3+} to Tb^{3+} and Tb^{3+} back to Dy^{3+} were controlled by selecting a suitable excitation wavelength, and the decay measurements were carried out for analyzing the energy transfer efficiency. These results indicate that the as-obtained phosphors could show merits of multicolor emissions in the visible region when excited by multi-wavelength light, which might find potential applications in the fields such as light display systems and watermarking technology.

Acknowledgements

This project is supported by the National Natural Science Foundation of China (No.21573142).

Notes and references

1 T. J. Mullen, M. Zhang, W. Feng, R. J. Elkhouri, L. D. Sun, C. H. Yan, T. E. Patten and G. Y. Liu, *ACS Nano.,* 2011**, 5,** 6539.

2 L. L. Han, Y. H. Wang, Y. Z. Wang, J. Zhang and Y. Tao, *J. Alloy. Compd.,* 2013**, 551**, 485.

3 (a) G. M. Cai, J. J. Fan, H. K. Li, Z. Zhao, L. M. Su and Z. P. Jin, *J. Alloy. Compd.,* 2013**, 562,** 182; (b) X. P. Chen, L. L. Zhang, Z. Q. Zhang, L. Zhu and W. C. Zhu, *CrystEngComm.,* 2015**, 17**, 7856.

4 X. A. Chen, Y. H. Zhao, X. Chang, J. L. Zuo, H. G. Zang and W. Q. Xiao, *J. Solid. State. Chem.,* 2006**, 179**, 3911.

5 P. X. Yan, J. Z. Liu, J. Wang and Z. G. Wu, *Appl. Phys. Lett.,* 2004**, 85**, 4747.

6 L. J. Qiao, X. Wang, and Z. H. Liu, *Mater. Res. Bull.,* 2015**, 70**, 75.

7 O. Annalakshmi, M. T. Jose, U. Madhusoodanan, J. Subramanian, B. Venkatraman, G. Amarendra and A. B. Mandal, *J. Lumin.,* 2014**, 146**, 295.

8 L. Del Longo, M. Ferrari, E. Zanghellini, M. Bettinelli, J. A. Capobianco, M. Montagna and F. Rossi, *J. Non-Cryst. Solids.,* 1998**, 231**, 178.

9 J. P. Liu, Y. Y. Li, X. T. Huang, Z. K. Li, G. Y. Li and H. B. Zeng, *Chem. Mater*., 2008, **20**, 250.

10 H. S. Huang and Z. H. Liu, *J. Lumin.,* 2013**, 140**, 114.

11 P. Liang and Z. H. Liu, *CrystEngComm*., 2016, **18**, 1311.

12 E. Erdoğmuş and E. Korkmaz, 2014**, 125**, 4098.

13 K. Linganna, V. B. Sreedhar and C. K. Jayasankar, *Mater. Res. Bull.,* 2015**, 67**, 196.

14 D. Y. Wang, T. M. Chen and B. M. Cheng, *Inorg. Chem.,* 2012**, 51**, 2961.

15 U. Caldiño, H. G. Muñoz, I. Camarillo, A. Speghini and M. Bettinelli, *J. Lumin.,* 2015**, 161**, 142.

16 A. Shyichuk and S. Lis, *Mater. Chem. and PhyS.,* 2013**, 140**, 447.

17 C. X. Qin, L. Qin, G. Q. Chen and T. Lin, *Mater Lett.,* 2013, **106**, 436.

18 M. Manhas, V. Kumar, G. Agarwal, O. M. Ntwaeaborwa and H. C. Swart, *Indian. J. Phys,.* 2015**, 89**, 899.

19 F. X. Shan, G. C. Zhang, X. Y. Zhang, T. X. Xu, Y. X. Wu, Y. Fu and Y. C. Wu, *J. Cryst. Growth.,* 2015**, 424**, 1.

20 J. Thakur, D. P. Dutta, H. Bagla and A. K. Tyagi, *J. Am. Ceram. Soc.,* 2012**, 95**, 696.

21 D. Y. Wang, Y. C. Chen, C. H. Huang, B. M. Cheng and T. M. Chen, *J. Mater. Chem.* 2012**, 22**, 9957.

22 J. Li, C. X. Zhang, Q. Tang, Y. L. Zhang, J. Q. Hao, Q. Su and S. B. Wang, *J. Phys. Chem. Solids.,* 2007**, 68**, 143.

23 H. H. Lin, G. B. Zhang, P. A. Tanner, H. B. Liang, *The J. Phys. Chem. C.,* 2013**, 117**, 12769.

24 M. M. Shang, C. X. Li and J. Lin, *Chem. Soc. Rev.,* 2014**, 43**, 1372.

25 (a) D. Tu, Y. J. Liang, R. Liu and D. Y. Li, *J. Lumin.,* 2011**, 131**, 2569; (b) S. Ghosh, K. Das, G. Sinha, J. Lahtinen and S. K. De, *J. Mater. Chem. C.,* 2013**, 1**, 5557; (c) H. Guo, F. Li, R. F. Wei, H. Zhang and C. G. Ma, *J. Am. Ceram. Soc.,* 2012**, 95**, 1178; (d) X. W. Zhang, Z. Zhao, X. Zhang, A. Marathe, D. B. Cordes, B. Weeks and J. Chaudhuri, *J. Mater. Chem. C.*, 2013, **1**, 7202.

26 Y. F. Yang, Y. Z. Jin, H. P. He, Q. L. Wang, Y. Tu, H. M. Lu and Z. Z. Ye, *J. Am. Chem. Soc.,* 2010**, 132**, 13381.

27 D. Yue, W. Lu, C. Y. Li, X. L. Zhang, C. X. Liu and Z. L. Wang, *Nanoscale.,* 2014**, 6**, 2137.

28 R. Zamiri, A. F. Lemos, A. Reblo, H. A. Ahangar, J. M. F. Ferreira, *Ceram. Int.,* 2014**, 40**, 523.

29 C. H. Zhang, H. B. Liang, S. Zhang, C. M. Liu, D. J. Hou, L. Zhou, G. B. Zhang and J. Y. Shi, *J. Phys. Chem. C.,* 2012**, 116**, 15932.

30 V. Mahalingam, J. Thirumalai, R. Krishnan and S. Mantha, *Spectrochim. Acta. A.,* 2016**, 152**, 172.

31 L. L. Li, R. Q. Li, W. W. Zi and S. C. Gan, *Physica. B.,* 2015**, 458**, 8.

32 H. B. Liang, Q. Zeng, Z. F. Tian, H. H. Lin, Q. Su, G. B. Zhang and Y. B. Fu, *J. Electrochem. Soc.,* 2007**, 154**, 177.

33 G. Seeta Rama Raju, E. Pavitra and J. S. Yu, *Phys.Chem. Chem. Phys.,* 2014**, 16**, 18124.

34 S. K. Gupta, V. Grover, R. Shukla, K. Srinivasu, V. Natarajan and A. K. Tyagi, *Chem. Eng. J.,* 2016**, 283**, 114.

35 Z. T. Yu, J. J. Xu, Y. S. Jiang, Z. Shi, Y. Guo, D. J. Wang and J. S. Chen, *J. Mater. Chem.,* 2003, **13**, 2227.

36 Y. Zhou, B. Yan and X. H. He, *J. Mater. Chem. C.,* 2014**, 2**, 848.

37 D. Ramachari, L. R. Moorthy and C. K. Jayasankar, *Ceram. Int.,* 2014**, 40**, 11115.

38 D. Yue, Q. F. Li, W. Lu, Q. Wang, M. N. Wang, C. Y. Li, L. Jin, Y. R. Shi, Z. L. Wang and J. H. Hao, *J. Mater. Chem. C.,* 2015**, 3**, 2865.

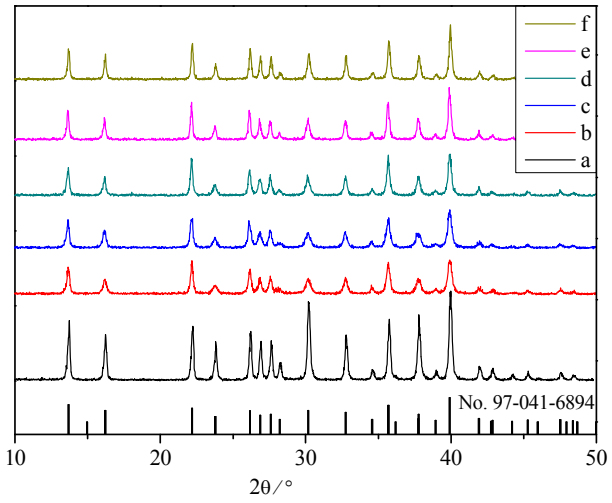

Fig. 1 XRD patterns of ZBH:xTb^{3+} at different concentrations: (a)x=0, (b)x=0.01, (c)x=0.03, (d)x=0.05, (e)x=0.07, (f)x=0.10 and the standard data for ZBH (JCPDS card no. 97-041-6894)

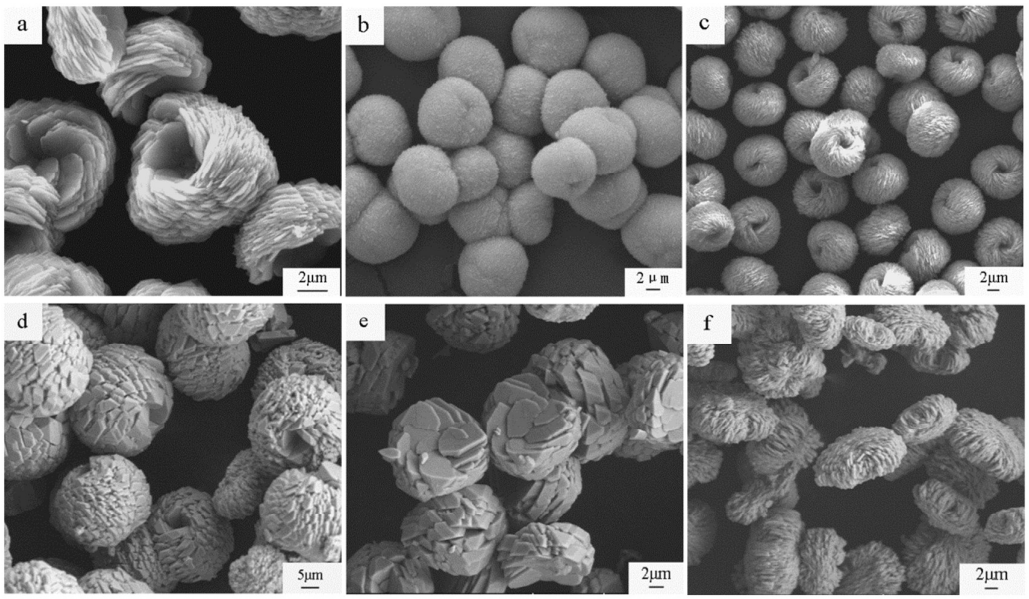

Fig. 2 SEM imagines of ZBH:xTb^{3+} at different concentrations: (a)x=0, (b)x=0.01, (c)x=0.03, (d)x=0.05, (e)x=0.07, (f)x=0.10

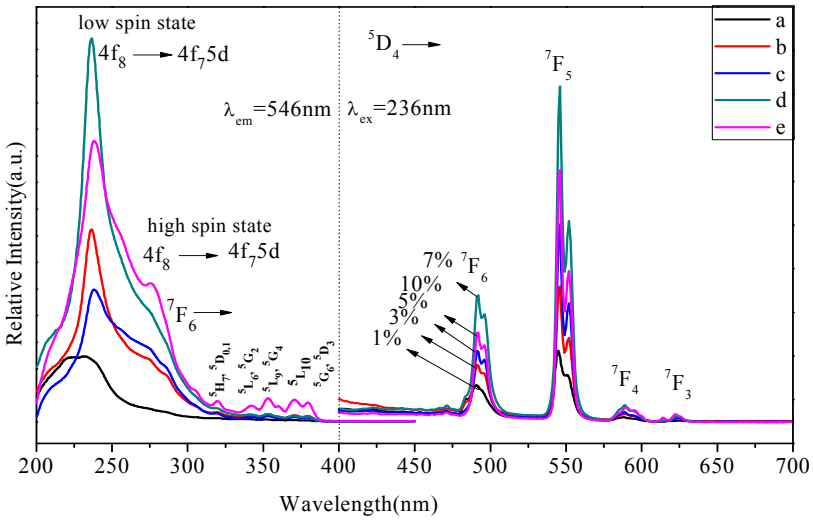

Fig. 3 PL excitation (left) and emission spectra (right) of ZBH:xTb^{3+} at different concentrations: (a)x=0.01, (b)x=0.03, (c)x=0.05, (d)x=0.07, (e)x=0.10

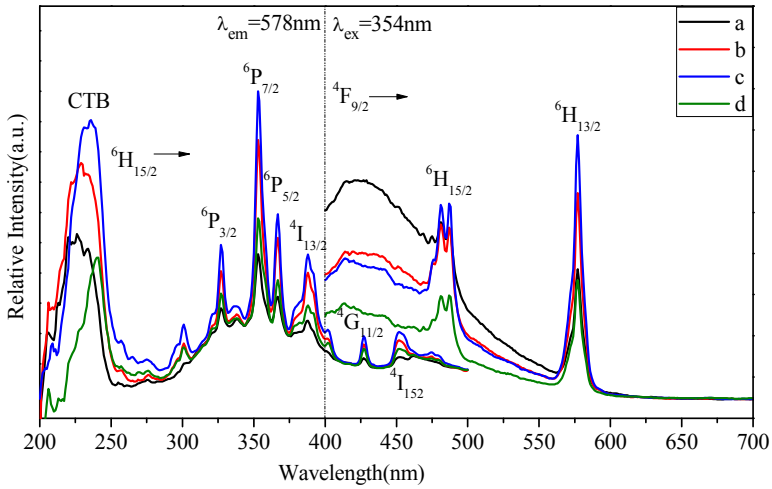

Fig. 4 PL excitation (left) and emission spectra (right) of ZBH:xDy^{3+} at different concentrations: (a)x=0.01, (b)x=0.02, (c)x=0.03, (d)x=0.04

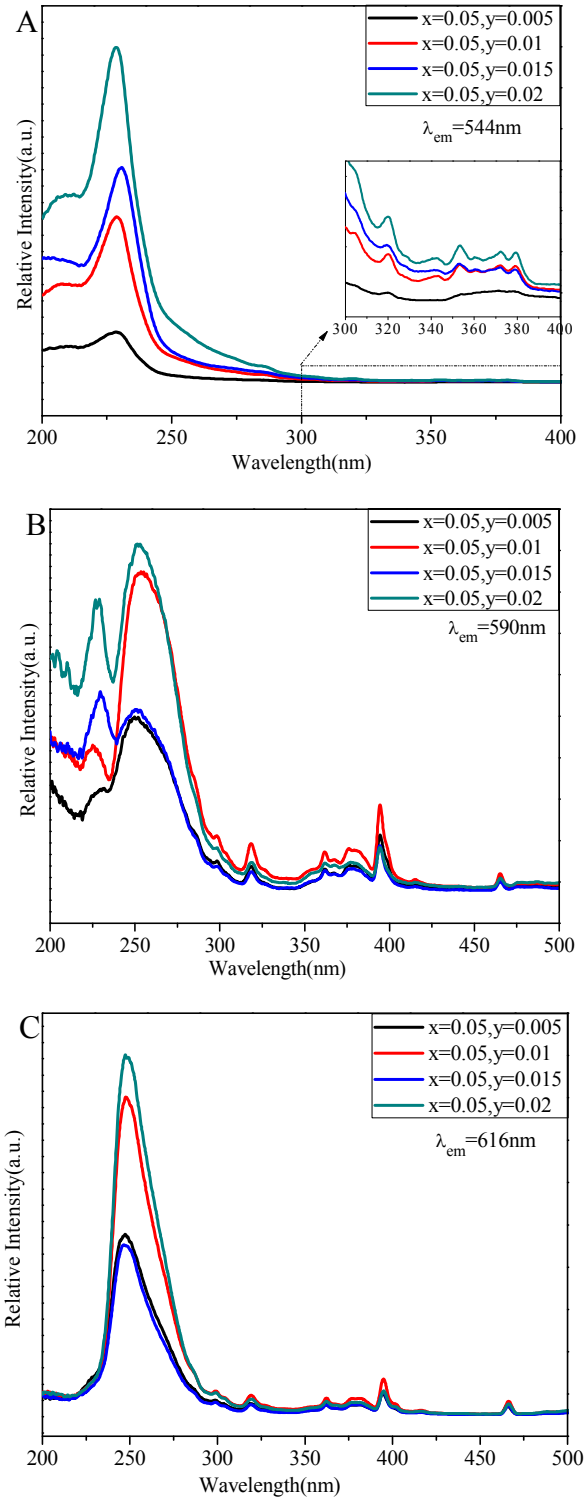

Fig. 5 Excitation spectra of ZBH:xEu^{3+}/yTb^{3+} (x=0.05; y=0.005, 0.01, 0.015 and 0.02) under the emission wavelength at 544 nm (A), 590 nm (B) and 616 nm (C), respectively.

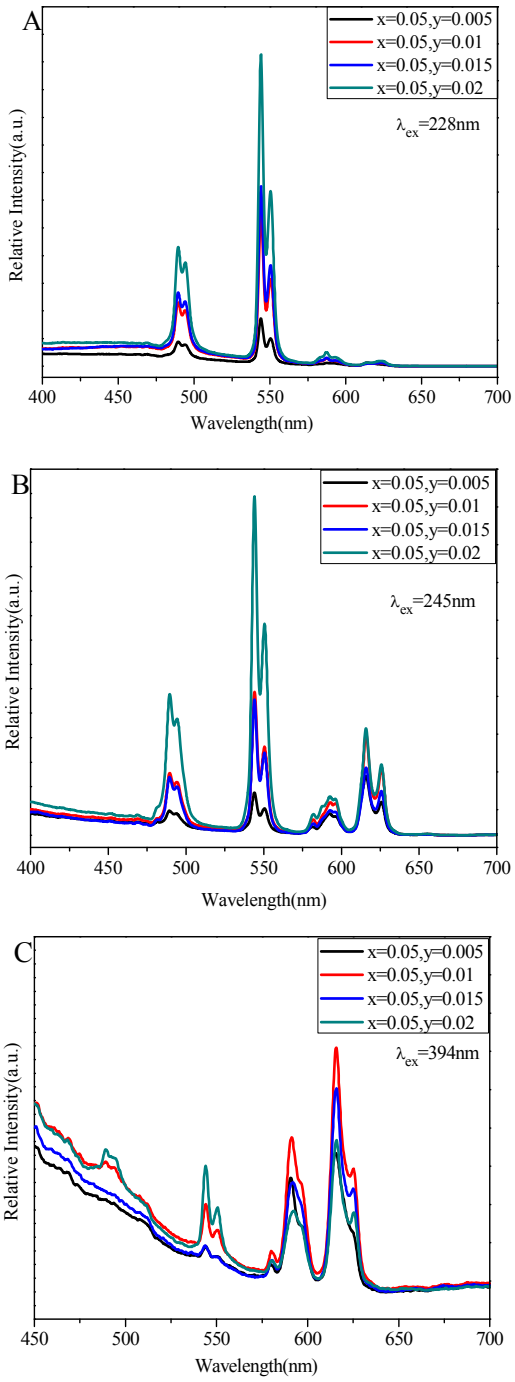

Fig. 6 Emission spectra of ZBH:xEu^{3+}/yTb^{3+} (x=0.05; y=0.005, 0.01, 0.015 and 0.02) excited at 228 nm (A), 245 nm (B) and 394 nm (C).

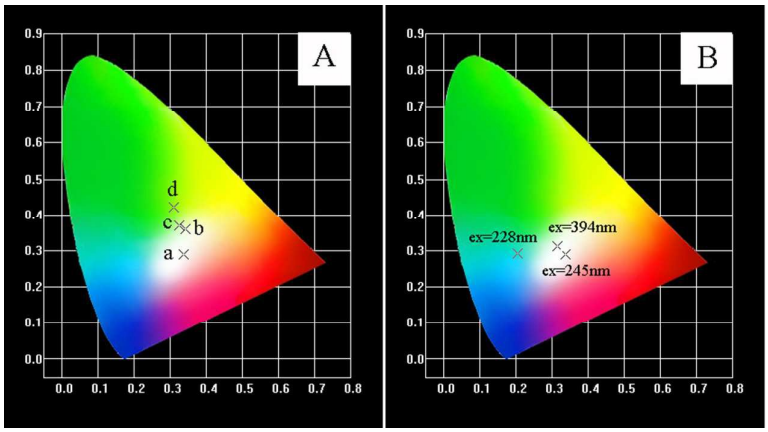

Fig. 7 (A) CIE diagram of ZBH:xEu^{3+}/yTb^{3+} (x=0.05; y=0.005 (a), 0.01 (b), 0.015 (c) and 0.02 (d)) excited at 245 nm and (B) ZBH:0.05Eu^{3+}/0.005Tb^{3+} excited at 228 nm, 245 nm and 394 nm, respectively.

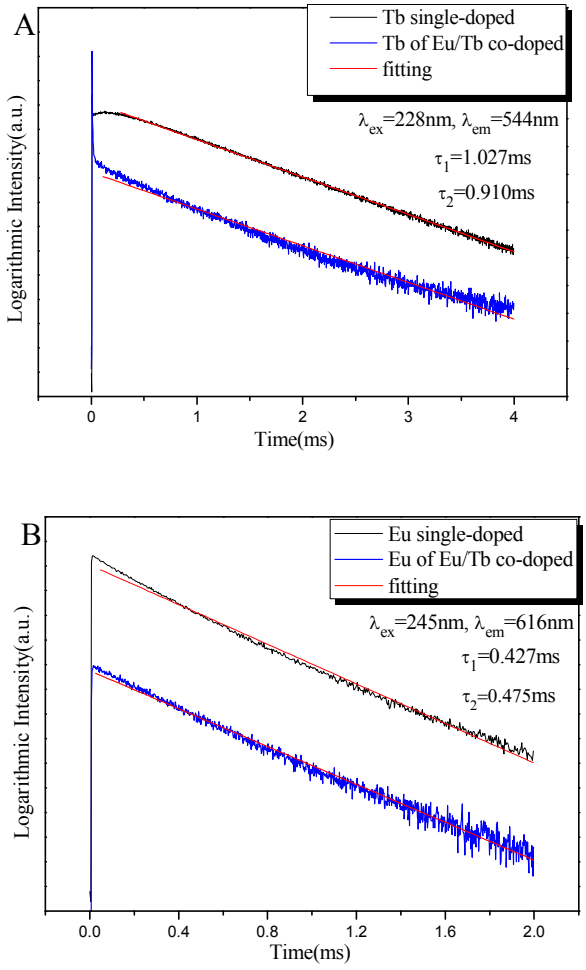

Fig. 8 Luminescent decay curve of (A)Tb^{3+} in ZBH:0.005Tb^{3+} (black curve) and ZBH:0.05Eu^{3+}/0.005Tb^{3+} (blue curve) and their fitting curves(red curves), (B)Eu^{3+} in ZBH:0.05Eu^{3+} (black curve) and ZBH:0.05Eu^{3+}/0.005Tb^{3+} (blue curve) and their fitting curves(red curves)

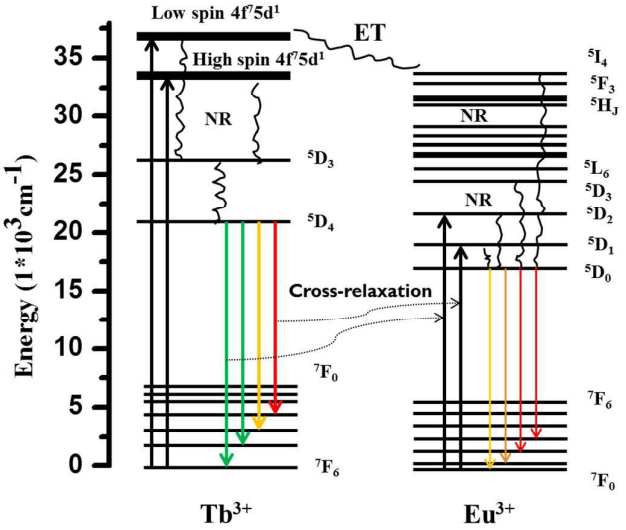

Fig. 9 Energy transfer scheme from Tb^{3+} to Eu^{3+} in ZBH: xEu^{3+}/yTb^{3+} (x=0.05; y=0.005, 0.01, 0.015 and 0.02)

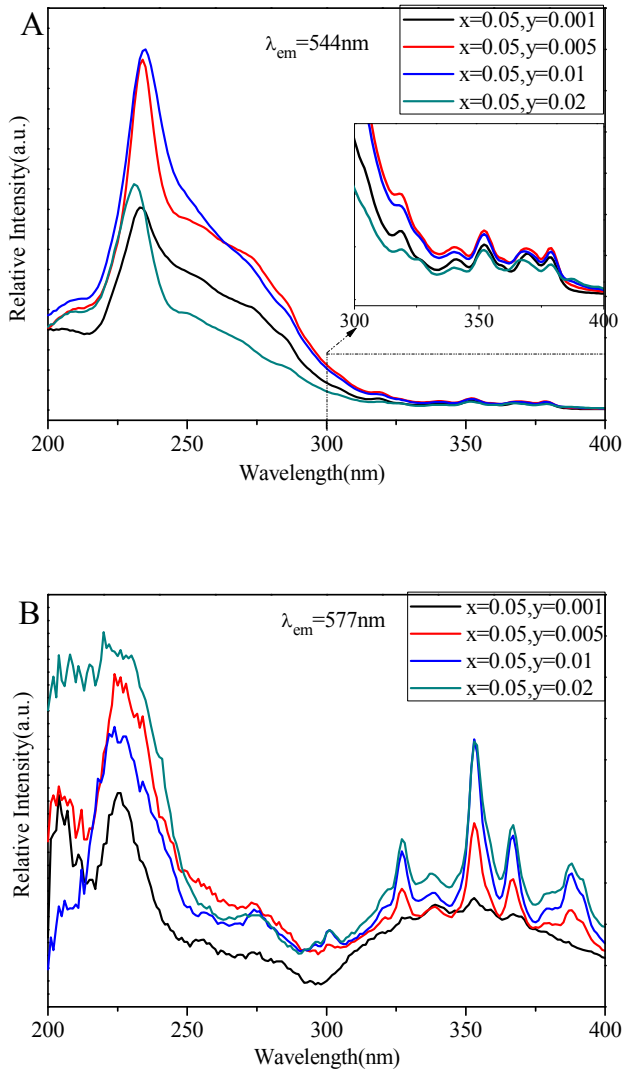

Fig. 10 Excitation spectra of ZBH:xTb^{3+}/yDy^{3+} (x=0.05; y=0.001, 0.005, 0.01 and 0.02) excited at 577 nm (A) and 544 nm (B)

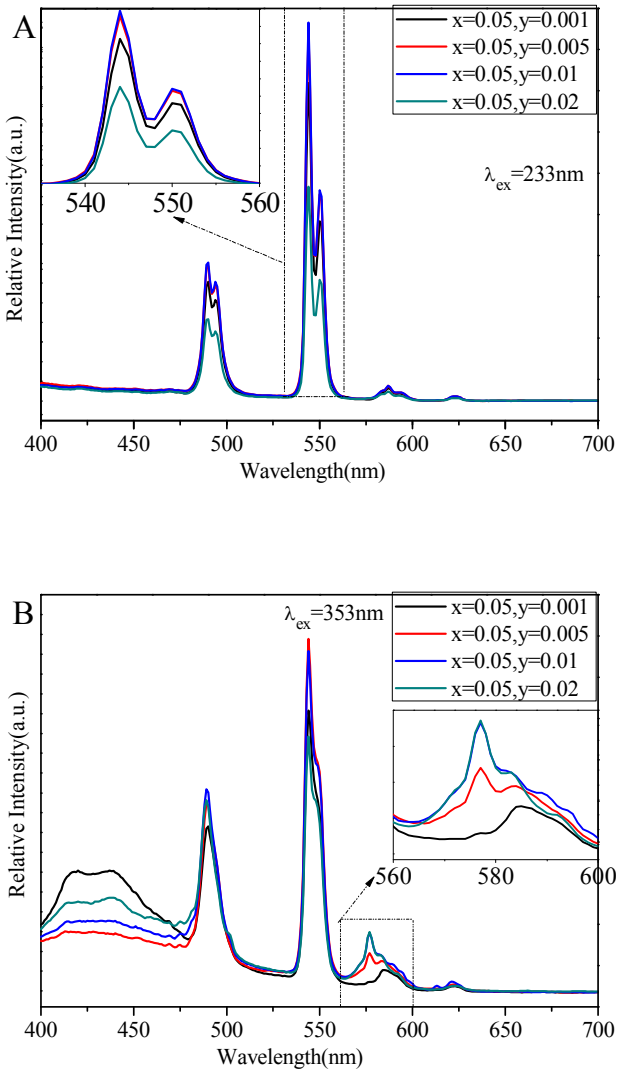

Fig. 11 Emission spectra of ZBH:xTb^{3+}/yDy^{3+} (x=0.05; y=0.001, 0.005, 0.01 and 0.02) excited at 233 nm (A) and 353 nm (B)

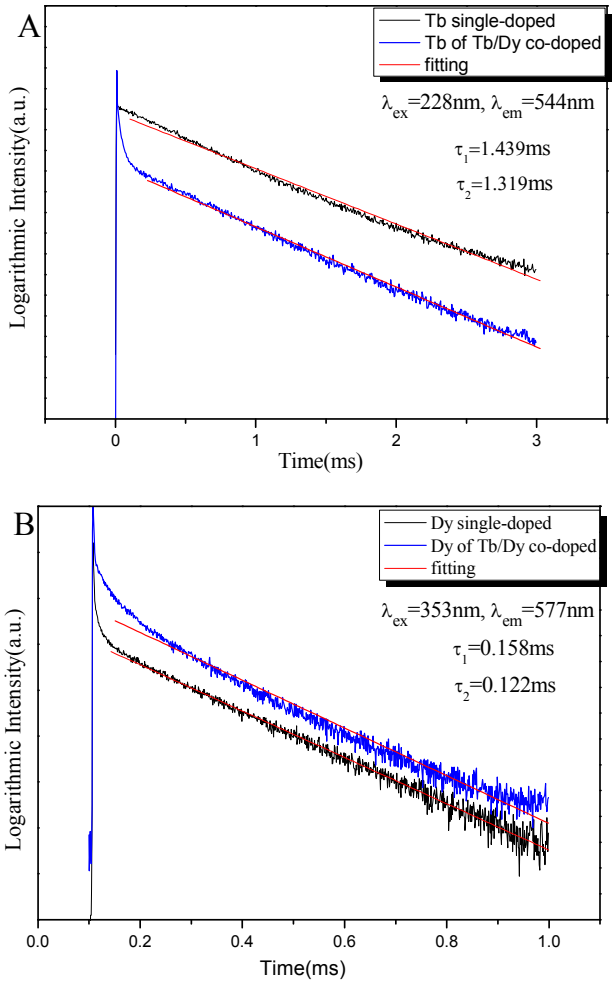

Fig. 12 (A) Luminescent decay curve of Tb^{3+} in ZBH:0.05Tb^{3+} (black curve) and ZBH:0.05Tb^{3+}/0.01Tb^{3+} (blue curve); (B) luminescent decay curve of Dy^{3+} in ZBH:0.05Tb^{3+} (black curve) and ZBH:0.05Tb^{3+}/0.01Tb^{3+} (blue curve) and their fitting curves (red curves)

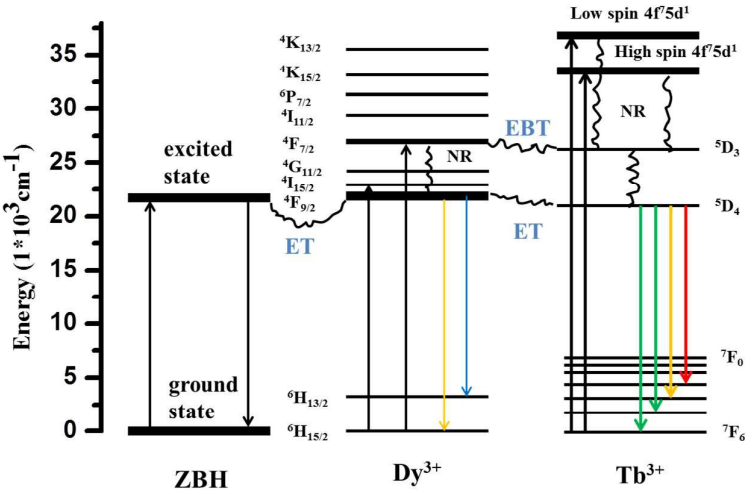

Fig. 13 Energy transfer scheme from host to Dy^{3+} and Tb^{3+} in ZBH: xTb^{3+}/yDy^{3+} (x=0.05; y=0.001, 0.005, 0.01 and 0.02)

Graphical Abstract

Controllable hydrothermal synthesis of $Eu^{3+}/Tb^{3+}/Dy^{3+}$ activated $Zn_8[(BO_3)_3O_2(OH)_3]$ micro/nanostructured phosphors: energy transfer and tunable emissions

P. Liang, J. W. Liu and Z. H. Liu*

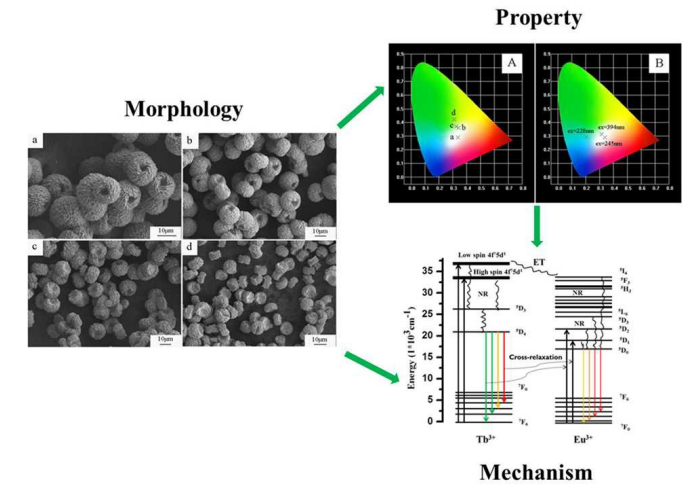

A series of novel Tb^{3+}, Dy^{3+} single-doped and Eu^{3+}/Tb^{3+}, Tb^{3+}/Dy^{3+} co-doped $Zn_8[(BO_3)_3O_2(OH)_3]$ (ZBH) micro/nanostructured phosphors have been prepared. When co-doped the Eu^{3+} and Tb^{3+} ions into the ZBH matrix, the phosphor yielded tunable emissions including tri-band established white light emission based on the co-doped concentration and excitation wavelength. The different concentration of rare earth doped in our system can change the composition and further change the morphology. The different composition and morphology can change their luminescence property through crystal field, center of luminescence, defects and other factors. The luminescence property is also related their luminescence mechanism.